

## Extraction of tight binding parameters from *in-situ* ARPES on the continuously doped surface of cuprates

YiGui Zhong<sup>1,2†</sup>, YiMeng Chen<sup>2†</sup>, JianYu Guan<sup>1,2</sup>, Jin Zhao<sup>1,2</sup>, ZhiCheng Rao<sup>1,2</sup>,  
CenYao Tang<sup>1,2</sup>, HaiJiang Liu<sup>1,2</sup>, YuJie Sun<sup>1</sup>, and Hong Ding<sup>1,2,3\*</sup>

<sup>1</sup> Beijing National Laboratory for Condensed Matter Physics and Institute of Physics, Chinese Academy of Sciences, Beijing 100190, China;

<sup>2</sup> School of Physics, University of Chinese Academy of Sciences, Beijing 100190, China;

<sup>3</sup> Collaborative Innovation Center of Quantum Matter, Beijing 100190, China

Received August 19, 2018; accepted September 17, 2018; published online October 18, 2018

Recently we developed a technique of ozone/vacuum annealing to continuously change the doping level of the surface of  $\text{Bi}_2\text{Sr}_2\text{CaCu}_2\text{O}_{8+x}$  and measured a nearly whole superconducting dome on one surface by *in-situ* angle-resolved photoemission spectroscopy [arXiv: 1805.06450]. Here we study the evolution of the electronic structures of  $\text{Bi}_2\text{Sr}_2\text{CaCu}_2\text{O}_{8+x}$  using this technique together with tight binding fits. The tight binding parameters are extracted to study their evolution with doping.

**cuprates, electronic structures, doping evolution, tight binding, ARPES**

**PACS number(s):** 74.72.Hs, 74.25.Jb, 79.60.-i

**Citation:** Y. G. Zhong, Y. M. Chen, J. Y. Guan, J. Zhao, Z. C. Rao, C. Y. Tang, H. J. Liu, Y. J. Sun, and H. Ding, Extraction of tight binding parameters from *in-situ* ARPES on the continuously doped surface of cuprates, *Sci. China-Phys. Mech. Astron.* **61**, 127403 (2018), <https://doi.org/10.1007/s11433-018-9305-y>

### 1 Introduction

The physics of high- $T_c$  cuprate superconductors is fascinating since a small variation of carrier doping can significantly change the electronic structure. For example, in the hole-doped cuprates a large hole-like Fermi surface that locates around the  $(\pi, \pi)$  points degenerates to an incomplete “Fermi arc” due to the widely studied pseudogap [1-4] in the underdoped (UD) region. Therefore, a systematic study of electronic structure evolution in a wide range of doping is critical to understand the superconducting mechanism of cuprates. However, surface cleaving, which is necessary for surface techniques such as angle-resolved photoemission spectroscopy (ARPES) and scanning tunneling spectroscopy (STS) that are powerful in revealing the electronic structure

of cuprates [5,6], poses a serious problem for quantitative comparisons from sample to sample due to the different conditions of the surfaces. Recently, we developed a new technique of ozone/vacuum annealing to continuously change the doping level of the surface layers of  $\text{Bi}_2\text{Sr}_2\text{CaCu}_2\text{O}_{8+x}$  ( $\text{Bi}2212$ ), which enables us to measure almost the whole superconducting dome on one sample surface by *in-situ* ARPES [7]. Here we use the single-band tight binding (TB) model to fit the electronic structure obtained by this technique, including Fermi surface (FS) and band structure. We obtain the TB parameters and their doping evolution, which are important for understanding the properties of cuprates [8].

### 2 Experimental methods

The surface treatments through ozone/vacuum annealing and

<sup>†</sup>These authors contributed equally to this work.  
<sup>\*</sup>Corresponding author (email: [dingh@iphy.ac.cn](mailto:dingh@iphy.ac.cn))

the sample preparation are described in our recent paper [7]. *In-situ* ARPES measurements were carried in an ARPES system equipped with a Scienta R4000 analyzer and a Scienta VUV source. A He I $\alpha$  resonant line ( $h\nu=21.218$  eV) was used, and the vacuum of the ARPES chamber was better than  $3\times 10^{-11}$  torr. The energy and angular resolution was set at  $\sim 20$  meV and  $0.2^\circ$ , respectively. All Fermi surface sheets were acquired at 30 K and integrated over  $\pm 10$  meV around the Fermi energy which was measured in a polished gold that is tightly contacted to with the sample and the ground.

### 3 Experimental results

Through a series of ozone and vacuum annealing, we obtained the FS sheets at different doped levels (Figure 1(a)-(h)). In principle the FS of Bi2212 is a distorted circle around the  $(\pi, \pi)$  point. However, in practice the FS of Bi2212 is more complicated: Firstly, as a result of the bilayer splitting [9], the main FS splits into the bonding FS branch and the anti-bonding FS branch as shown in Figure 1(a); Secondly,

there are several of “ghost” FS sheets due to the Bi-O superlattice modulation, and a “shadow” FS sheet stemmed from the orthorhombic folding as illustrated in Figure 1(a). We apply a single-band TB model plus a bilayer splitting term to fit the FS sheets with the constraint  $t''/t'=-1/2$  as suggested previously [8,10-12]. In order to make the fitting robust and comparable, we scale all TB parameters to the value of the first-nearest-neighbor hopping integral  $t$  (eq. (1)).

$$E(k_x, k_y) = \mu / t + \frac{1}{2}(\cos k_x a + \cos k_y a) + t' / t \cos k_x a \cos k_y a + \frac{1}{2} t'' / t (\cos 2k_x a + \cos 2k_y a) \pm \frac{t_{\text{bi}}}{4t} (\cos k_x a - \cos k_y a)^2. \quad (1)$$

The fittings are based on the  $k_f$  points defined as the minimum gap locus shown as the red points (bonding) and black points (anti-bonding) in Figure 1(a)-(h). One can see that the fitting FS contours match well with those  $k_f$  points or the underlying FS sheets, including the main FS sheets, the superlattice FS sheets, and even the weak shadow FS sheet

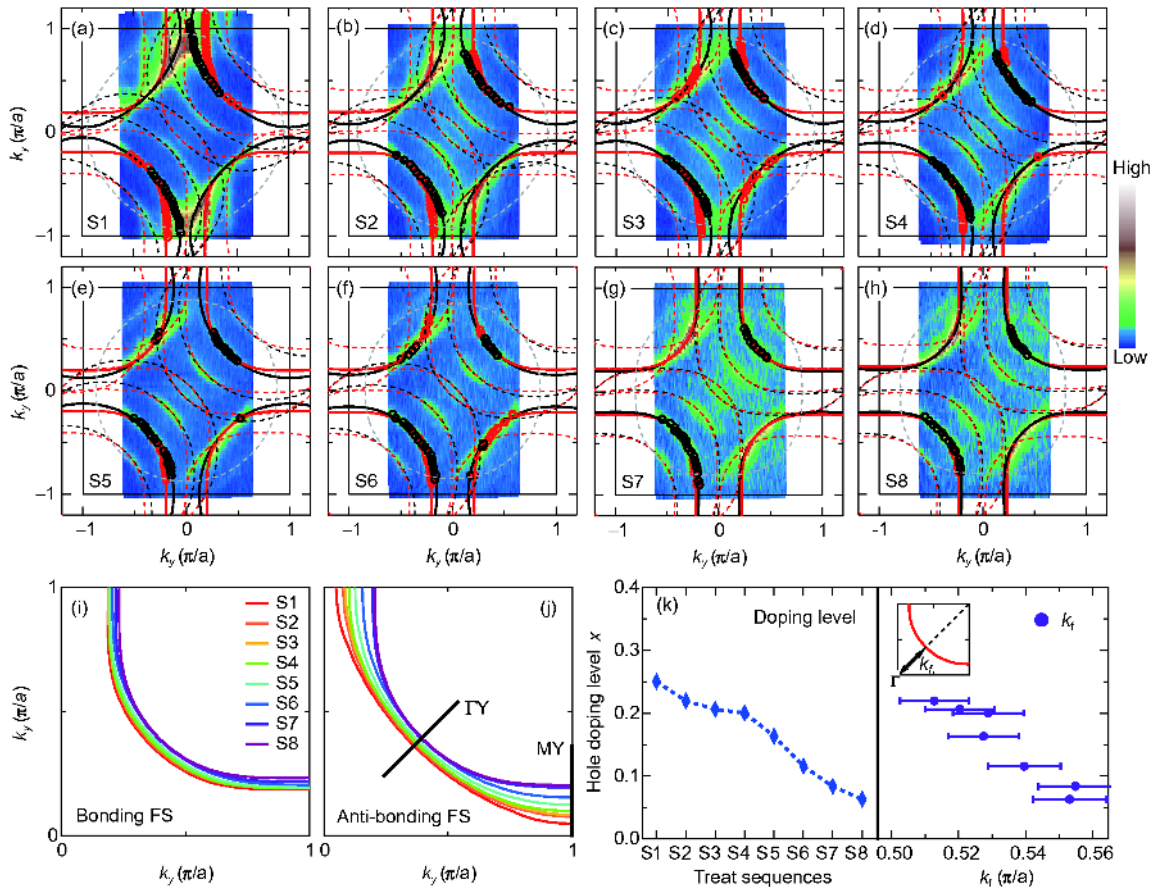


**Figure 1** (Color online) Doping evolution of Fermi surface. (a)-(h) Fermi surfaces of each treat sequence; (a) Fermi surface acquired by ozone annealing; (b)-(h) Fermi surfaces of a series of vacuum annealing. The solid red lines and black lines represent the bonding FS contours and antibonding FS contours from TB fit, respectively. Dash red lines are the superlattice FS contours and the gray dash lines are the shadow FS contours. The red or black circles are the  $k_f$  points with a minimum excitation gap along the bonding or anti-bonding FS. (i), (j) Doping evolution of bonding FS and anti-bonding FS contours. The doping levels of them are marked with the blue diamonds in the left panel of (k). The nodal  $k_f$  relative to the  $\Gamma$  point is plotted in the right panel of (k).

(Figure 1(a)-(h)). We summarize the fitting bonding FS and anti-bonding FS contours at different doping levels shown in Figure 1(i) and (j), respectively. It is evident that the FS shrinks and the nodal  $k_f$  point smoothly moves toward the center of the hole FS (Figure 1(k)), which is consistent with a reduction of the doping level. It is well established that the relative area of a FS to the Brillouin zone equals or is equal to  $(1+x)/2$ , where  $x$  is the doped concentration [7], so we can get the doping level of each annealing sequence from the area of fitted FS contours as plotted in the left panel of Figure 1(k).

In Figure 2 we plot the doping evolution of the scaled TB parameters. We find that the chemical potential  $\mu/t$  shifts to the zero energy with the decreasing of doping concentration as shown in Figure 2(a). In a hole-like rigid-band system, the chemical potential would gradually shift to the top of the band when holes are taken away from the material. We also find that the value of  $t_{\text{bi}}/4t$ , which represents the extent of bilayer splitting, decays linearly as doping is reduced (Figure 2(b)), which is consistent with a previous observation [13]. We then evaluate the evolution of the second-nearest-neighbor hopping parameter  $t'/t$  in Figure 2(c) and (d). First of all, it seems to be slightly proportional to  $T_c$  as shown in Figure 2(d), here  $T_c$  is estimated from the doped concentration  $x$  according to the empirical formula of Bi2212

[14]. Since it has been suggested that  $t'/t$  is proportional to  $T_{c,\text{max}}$  in the cuprates [8,15], we plot  $t'/t$  versus  $T_{c,\text{max}}$  for several typical cuprate superconductors in Figure 2(d) for comparison. One can find that  $t'/t$  of Bi2212 has an opposite trend and a much smaller variation, which is about 20% of the optimal doped level.

In order to obtain the value of the first-nearest-neighbor hopping parameter  $t$ , we use the TB model to fit the band dispersion based on these scaled parameters. We focus on two principle directions, the MY direction which reflects the information of the antinodal region and the  $\Gamma Y$  direction which reflects the information of the nodal region. Their corresponding band positions in  $k$ -space are plotted in Figure 1(j). In this experiment we aligned the sample paralleling to the MY direction, so the band dispersion along MY was acquired in a direct way, while the dispersion along  $\Gamma Y$  was obtained indirectly from the spectral intensity  $I(E, k_x, k_y)$ . We fit the dispersion along MY first. The spectra along MY was measured above  $T_c$  or  $T_c^*$  (for UD region) and divided by the Fermi-Dirac function to avoid the large superconducting gap (or the pseudogap) and the associated band bending [16]. Since a highly overdoped sample has a well-defined band dispersion (Figure 3(a)), it is more reliable to determine the parameter  $t$  by fitting the MY band dis-

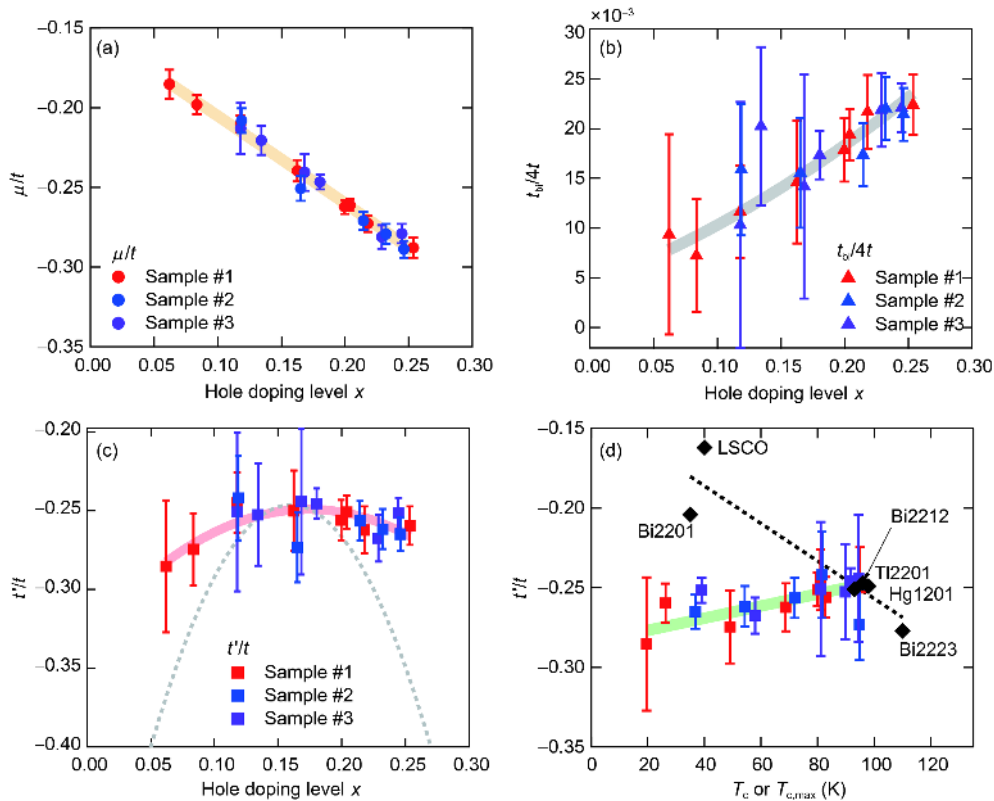


**Figure 2** (Color online) Doping evolution of TB fitting parameters. (a)-(c) Doping evolution of the scaled chemical potential  $\mu/t$ , interlayer hopping parameter  $t_{\text{bi}}/4t$ , and second-nearest-neighbor hopping integral  $t'/t$ ; three independent samples are marked with different colors, the red, blue, and violet, respectively. (d)  $t'/t$  evolution with  $T_c$ , which is calculated by the doped carrier concentration  $x$  according to the empirical formula of Bi2212 [14]. The black diamond one marks the values of  $t'/t$  of optimal doped LSCO, Bi2201, Bi2212, Tl2201, Hg1201 and Bi2223 plotted against with their  $T_{c,\text{max}}$ , the dash line is the linear fitting. These  $t'/t$  of different materials are from the ref. [15].

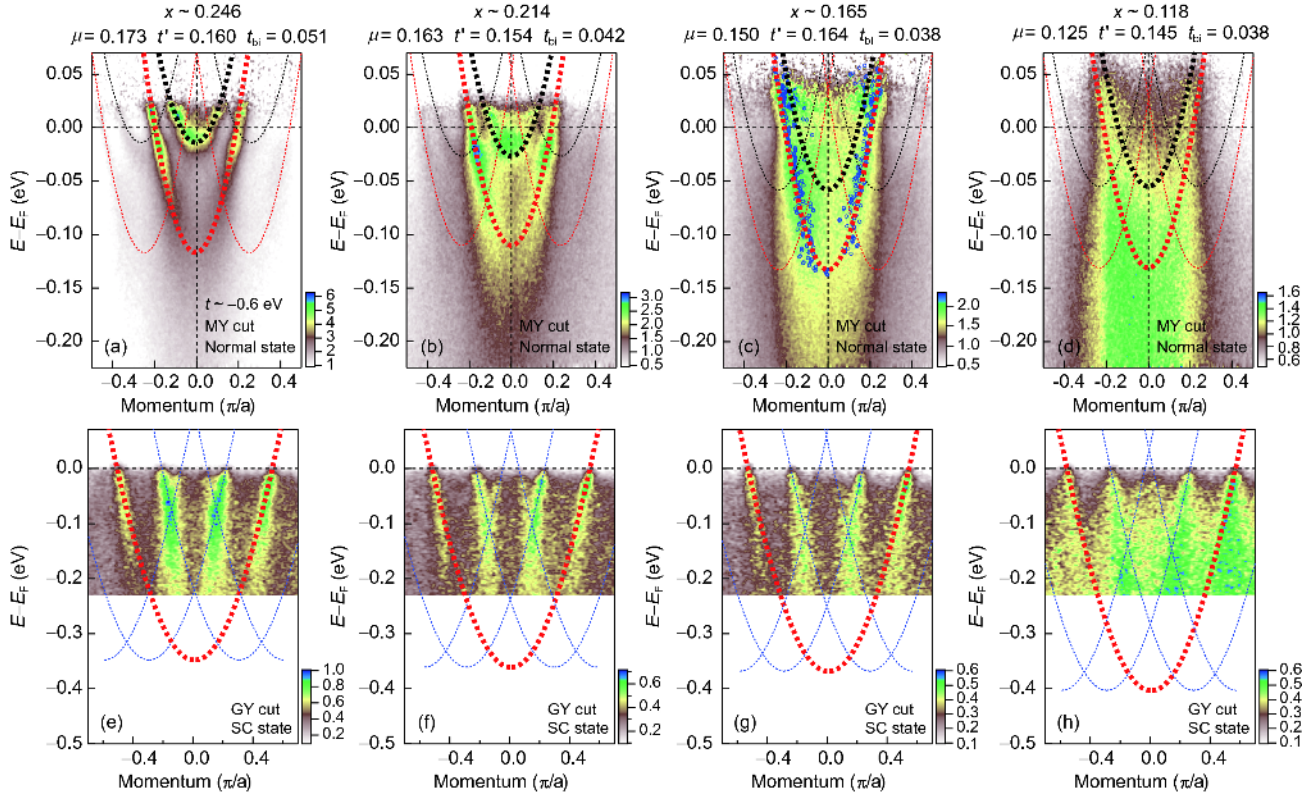


**Figure 3** (Color online) TB bands for  $x \sim 0.246, 0.214, 0.165, 0.118$  of sample #2. We fit the MY band of  $x \sim 0.246$ , and obtain the value of  $t$  of  $\sim -0.6$  eV as shown in (a); the thick black dash line is the fitting results of anti-bonding band and the thick red dash line is the fitting results of bonding band. (b)-(d) The TB bands calculated using  $t \sim -0.6$  eV and the parameter sets (unit in eV) listed on the top of images for each doping level along MY. The blue hollow circles in (c) are the peaks of the momentum dispersion curves. (e)-(h) The TB bands at GY direction. All thin dash lines in the figures are the corresponding superlattice bands for (a)-(h). The corresponding intensity color scale of each image is given in their low right.

persion of the highest overdoping level, which gives  $\sim -0.6$  eV. We assume the value of  $t$  is a constant for each doping level, and plot the corresponding TB bands for each doping level in Figure 3(b)-(h). For the MY direction, one can see that the band structure matches well with the TB band except for the ones in the UD region. This deviation might be due to the stronger electron correlations in the UD region. For the GY direction, the TB band also matches well with the main band and superlattice bands for the binding energy smaller than the energy of  $\sim 70$  meV, which is the energy position of the well-known kink for Bi2212 [17-20] as shown in Figure 3(e)-(h). The band dispersion along GY was measured in the superconducting state since the superconducting gap is zero along this direction. The Fermi velocity  $V_f$  derived from the TB fit along this direction is a constant,  $\sim -2$  eV  $\text{\AA}^{-1}$ , for every doping level, which is consistent with the previous results [21].

## 4 Discussion

As suggested previously [8], the value of  $t'/t$  is controlled by the crystal structure and the chemical composition, and the materials with larger  $t'/t$  tend to have higher values of  $T_{c,\max}$ .

For Bi2212, there is no change of the crystal structure when carriers are doped into the material, since the variation of symmetry and FS topology are not observed. We suspect that the change of chemical composition due to doped carriers is responsible for the 20% variation of  $t'/t$ . Even though the one with larger value of  $t'/t$  in the UD region tends to achieve higher value of  $T_c$ , the reduction of carrier concentration in this region still dominate the change of  $T_c$ . For cuprate superconductors, the superfluid density is believed to determine the value of  $T_c$  in the UD region [22]. Ding et al. [23] and Feng et al. [24] suggested that the doped carrier concentration of the UD region is closely related to the superfluid below  $T_c$ , which means that the decrease of carrier concentrations makes the system to have a lower value of  $T_c$ .

We notice that the TB band does not match well with the measured bands along MY direction in the UD region (Figure 3(c) and (d)). Since the normal state is a strange metal phase in this region, we speculate that this mismatch might be related to some kind of exotic behaviors of this strange metal phase.

For the GY direction, the fitted TB band has a good match with the measured band in the low binding energy for each doping, and starts to deviate at the binding energy higher than  $\sim 70$  meV due to the prominent dispersion kink [17-20].

The TB band has a constant Fermi velocity,  $-2 \text{ eV \AA}^{-1}$ , which is consistent with previous results [21]. However, a recent report [25] gave a smaller Fermi velocity  $V_f$  extracted within a very low energy window (0-7 meV below the Fermi energy), and it decreases with decreasing doping, while the band velocity of the intermediate binding energy (30-40 meV) remains a constant value ( $-2 \text{ eV \AA}^{-1}$ ) at different doping levels. If this variable  $V_f$  is used to estimate the value of  $t$ , then  $t$  would become smaller and smaller with decreasing doping, and the evolution of the chemical potential  $\mu$  and the interlayer hopping parameter  $t_{bi}$  will be unreasonable. The conclusion that the low energy kink at  $\sim 10 \text{ meV}$  stemming from the couplings with a low-energy mode [26,27] would be reconcile for this contradiction. Due to this low energy kink, the strong renormalization effect that is not included in the TB band changes the Fermi velocity in the UD region. The TB band parameters obtained here can be considered as the “bared band” which can be directly used in various theoretical models.

## 5 Conclusions

In conclusion, we present the evolution of the electronic structure of Bi2212 within a nearly whole superconducting dome by measuring on a continuously doped surface of Bi2212 using *in-situ* ARPES. By applying the single-band TB model to fit the FS sheets and the band structures, we determine the values of TB parameters and their evolution with doping, which are important for theoretical modeling of high- $T_c$  cuprates.

*This work was supported by the Ministry of Science and Technology of China (Grant Nos. 2016YFA0401000, 2016YFA0300600, 2015CB921300, and 2015CB921000), the National Natural Science Foundation of China (Grant Nos. 11227903, and 11574371), and the Chinese Academy of Sciences (Grant Nos. XDB07000000, and XDPB08-1).*

- 1 H. Ding, T. Yokoya, J. C. Campuzano, T. Takahashi, M. Randeria, M. R. Norman, T. Mochiku, K. Kadowaki, and J. Giapintzakis, *Nature* **382**, 51 (1996).
- 2 A. G. Loeser, Z. X. Shen, D. S. Dessau, D. S. Marshall, C. H. Park, P. Fournier, and A. Kapitulnik, *Science* **273**, 325 (1996).
- 3 S. Hüfner, M. A. Hossain, A. Damascelli, and G. A. Sawatzky, *Rep. Prog. Phys.* **71**, 062501 (2008), arXiv: 0706.4282.
- 4 T. Timusk, and B. Statt, *Rep. Prog. Phys.* **62**, 61 (1999).
- 5 A. Damascelli, Z. Hussain, and Z. X. Shen, *Rev. Mod. Phys.* **75**, 473 (2003).
- 6 Ø. Fischer, M. Kugler, I. Maggio-Aprile, C. Berthod, and C. Renner, *Rev. Mod. Phys.* **79**, 353 (2007).
- 7 Y. G. Zhong, J. Y. Guan, X. Shi, J. Zhao, Z. C. Rao, C. Y. Tang, H. J. Liu, G. D. Gu, Z. Y. Weng, Z. Q. Wang, T. Qian, Y. J. Sun, and H. Ding, arXiv: 1805.06450.
- 8 E. Pavarini, I. Dasgupta, T. Saha-Dasgupta, O. Jepsen, and O. K. Andersen, *Phys. Rev. Lett.* **87**, 047003 (2001).
- 9 D. L. Feng, N. P. Armitage, D. H. Lu, A. Damascelli, J. P. Hu, P. Bogdanov, A. Lanzara, F. Ronning, K. M. Shen, H. Eisaki, C. Kim, Z. X. Shen, J. I. Shimoyama, and K. Kishio, *Phys. Rev. Lett.* **86**, 5550 (2001).
- 10 M. Hashimoto, T. Yoshida, H. Yagi, M. Takizawa, A. Fujimori, M. Kubota, K. Ono, K. Tanaka, D. H. Lu, Z. X. Shen, S. Ono, and Y. Ando, *Phys. Rev. B* **77**, 094516 (2008), arXiv: 0801.0782.
- 11 T. Yoshida, X. J. Zhou, K. Tanaka, W. L. Yang, Z. Hussain, Z. X. Shen, A. Fujimori, S. Sahrakorpi, M. Lindroos, R. S. Markiewicz, A. Bansil, S. Komiya, Y. Ando, H. Eisaki, T. Kakeshita, and S. Uchida, *Phys. Rev. B* **74**, 224510 (2006).
- 12 R. S. Markiewicz, S. Sahrakorpi, M. Lindroos, H. Lin, and A. Bansil, *Phys. Rev. B* **72**, 054519 (2005).
- 13 T. K. Kim, A. A. Kordyuk, S. V. Borisenko, A. Koitzsch, M. Knupfer, H. Berger, and J. Fink, *Phys. Rev. Lett.* **91**, 167002 (2005).
- 14 M. R. Presland, J. L. Tallon, R. G. Buckley, R. S. Liu, and N. E. Flower, *Physica C* **176**, 95 (1991).
- 15 W. S. Lee, T. Yoshida, W. Meevasana, K. M. Shen, D. H. Lu, W. L. Yang, X. J. Zhou, X. Zhao, G. Yu, Y. Cho, M. Greven, Z. Hussain, and Z. X. Shen, arXiv: preprint cond-mat/0606347.
- 16 M. Hashimoto, I. M. Vishik, R. H. He, T. P. Devereaux, and Z. X. Shen, *Nat. Phys.* **10**, 483 (2014), arXiv: 1503.00391.
- 17 A. Lanzara, P. V. Bogdanov, X. J. Zhou, S. A. Kellar, D. L. Feng, E. D. Lu, T. Yoshida, H. Eisaki, A. Fujimori, K. Kishio, J. I. Shimoyama, T. Noda, S. Uchida, Z. Hussain, and Z. X. Shen, *Nature* **412**, 510 (2001).
- 18 P. D. Johnson, T. Valla, A. V. Fedorov, Z. Yusof, B. O. Wells, Q. Li, A. R. Moodenbaugh, G. D. Gu, N. Koshizuka, C. Kendziora, S. Jian, and D. G. Hinks, *Phys. Rev. Lett.* **87**, 177007 (2001).
- 19 T. P. Devereaux, T. Cuk, Z. X. Shen, and N. Nagaosa, *Phys. Rev. Lett.* **93**, 117004 (2004).
- 20 M. Eschrig, and M. R. Norman, *Phys. Rev. B* **67**, 144503 (2003).
- 21 X. J. Zhou, T. Yoshida, A. Lanzara, P. V. Bogdanov, S. A. Kellar, K. M. Shen, W. L. Yang, F. Ronning, T. Sasagawa, T. Kakeshita, T. Noda, H. Eisaki, S. Uchida, C. T. Lin, F. Zhou, J. W. Xiong, W. X. Ti, Z. X. Zhao, A. Fujimori, Z. Hussain, and Z. X. Shen, *Nature* **423**, 398 (2003).
- 22 J. L. Tallon, J. W. Loram, J. R. Cooper, C. Panagopoulos, and C. Bernhard, *Phys. Rev. B* **68**, 180501 (2003).
- 23 H. Ding, J. R. Engelbrecht, Z. Wang, J. C. Campuzano, S. C. Wang, H. B. Yang, R. Rogan, T. Takahashi, K. Kadowaki, and D. G. Hinks, *Phys. Rev. Lett.* **87**, 227001 (2001).
- 24 D. L. Feng, D. H. Lu, K. M. Shen, C. Kim, H. Eisaki, A. Damascelli, R. Yoshizaki, J. Shimoyama, K. Kishio, G. D. Gu, S. Oh, A. Andrus, J. O'Donnell, J. N. Eckstein, and Z. X. Shen, *Science* **289**, 277 (2000).
- 25 I. M. Vishik, W. S. Lee, F. Schmitt, B. Moritz, T. Sasagawa, S. Uchida, K. Fujita, S. Ishida, C. Zhang, T. P. Devereaux, and Z. X. Shen, *Phys. Rev. Lett.* **104**, 207002 (2010), arXiv: 1002.2630.
- 26 N. C. Plumb, T. J. Reber, J. D. Koralek, Z. Sun, J. F. Douglas, Y. Aiura, K. Oka, H. Eisaki, and D. S. Dessau, *Phys. Rev. Lett.* **105**, 046402 (2010), arXiv: 0903.4900.
- 27 T. Kondo, Y. Nakashima, W. Malaeb, Y. Ishida, Y. Hamaya, T. Takeuchi, and S. Shin, *Phys. Rev. Lett.* **110**, 217006 (2013), arXiv: 1212.0335.